Journal of Biomedical Informatics 63 (2016) 366–378

Contents lists available at ScienceDirect

Journal of Biomedical Informatics

journal homepage: www.elsevier.com/locate/yjbin

A model-driven methodology for exploring complex disease comorbidities applied to autism spectrum disorder and inflammatory bowel disease

Judith Somekh [a,b,*], Mor Peleg [b], Alal Eran [a,i,j], Itay Koren [c,d,e], Ariel Feiglin [a], Alik Demishtein [f], Ruth Shiloh [g], Monika Heiner [h], Sek Won Kong [i], Zvulun Elazar [f], Isaac Kohane [a]

[a] Department of Biomedical Informatics, Harvard Medical School, Boston, MA, USA
[b] Department of Information Systems, University of Haifa, Haifa, Israel
[c] Department of Genetics, Harvard Medical School, Boston, MA, USA
[d] Division of Genetics, Brigham and Women's Hospital, Boston, MA, USA
[e] Howard Hughes Medical Institute, Boston, MA, USA
[f] Department of Biological Chemistry, Weizmann Institute of Science, Rehovot, Israel
[g] Department of Molecular Genetics, Weizmann Institute of Science, Rehovot, Israel
[h] Computer Science Institute, Brandenburg University of Technology, Cottbus, Germany
[i] Computational Health Informatics Program, Boston Children's Hospital, Boston, MA, USA
[j] Department of Life Sciences, Ben Gurion University of the Negev, Beer-Sheva, Israel

ARTICLE INFO

Article history:
Received 29 January 2016
Revised 29 July 2016
Accepted 5 August 2016
Available online 10 August 2016

Keywords:
Petri nets
Modeling
Autism
IBD
ASD
Autophagy

ABSTRACT

We propose a model-driven methodology aimed to shed light on complex disorders. Our approach enables exploring shared etiologies of comorbid diseases at the molecular pathway level. The method, Comparative Comorbidities Simulation (CCS), uses stochastic Petri net simulation for examining the phenotypic effects of perturbation of a network known to be involved in comorbidities to predict new roles for mutations in comorbid conditions. To demonstrate the utility of our novel methodology, we investigated the molecular convergence of autism spectrum disorder (ASD) and inflammatory bowel disease (IBD) on the autophagy pathway. In addition to validation by domain experts, we used formal analyses to demonstrate the model's self-consistency. We then used CCS to compare the effects of loss of function (LoF) mutations previously implicated in either ASD or IBD on the autophagy pathway. CCS identified similar dynamic consequences of these mutations in the autophagy pathway. Our method suggests that two LoF mutations previously implicated in IBD may contribute to ASD, and one ASD-implicated LoF mutation may play a role in IBD. Future targeted genomic or functional studies could be designed to directly test these predictions.

1. Introduction

Understanding the mechanisms underlying complex diseases is a central challenge of modern biomedical research. Comorbid diseases, i.e., those that co-occur in individuals or families, may point to partially overlapping etiologies.

Recent work demonstrates that comorbidity is significantly related to genetic similarity [1]. Melamed et al. [1] proposed a statistical approach to discover new cancer genes based on genetic similarity of comorbid pairs of Mendelian disease and cancers with shared cellular processes. Network-based approaches [e.g., 2,3] used large scale protein interaction networks to explore the convergence of protein interaction networks between comorbid diseases.

Toward the goal of utilizing comorbidities to identify novel complex disease genes, we developed a new approach – Comparative Comorbidities Simulation (CCS). CCS uses stochastic Petri net (SPN) simulation for examining the actual and potential phenotypic effects of perturbation of a network known to be involved in comorbidities to predict new roles for genes in the comorbid conditions. SPN is a mathematical formalism [4,5] where stochastic time-delays are assigned to each system event (e.g., enzymatic reaction) during simulation, enabling generation of dynamic behavior. We applied our approach to explore the molecular con-

* Corresponding author at: Department of Biomedical Informatics, Harvard Medical School, Boston, MA, USA.
E-mail address: judith_somekh@hms.harvard.edu (J. Somekh).

http://dx.doi.org/10.1016/j.jbi.2016.08.008
1532-0464/

vergence of autism spectrum disorder and inflammatory bowel disorder.

In addition, our model-driven approach aims to advance the understanding of similar mechanisms underlying comorbidities and to generate predictions that may help to identify genes for testing in order to further decipher the pathophysiology of comorbid diseases. We used CCS to examine the phenotypic effects of perturbation of a network that represents a biological process/-pathway known to be involved in both comorbidities. We propose that comparing the simulated behavior of perturbations corresponding to susceptible genes known to be associated with the comorbidities could uncover additional clues regarding their mechanisms of action.

CCS includes three steps, as shown in Fig. 1. First, we identify a pair of comorbid complex diseases and their candidate-shared processes/pathways are examined.

In the second step, we create a model of the biological process, including the disease-associated genes, using SPN. Our model is validated by domain experts, as well as by formal verification of desired invariants that should hold for biological pathways [4,5,6]. We further validate that simulating loss of function (LoF) mutations of interest complies with known experimental findings.

The third step includes comparing the *in silico* results and generating predictions of potential involvement of risk genes that are known to be related to the selected pathway. Such predictions could focus the research on new target genes to be tested to determine if they induce the comorbid disease.

We demonstrated our methodology on ASD and its IBD comorbidity. We have chosen these diseases because they are highly heritable comorbid conditions of mostly unknown etiologies, whose comorbidity may hint at their underlying molecular alterations. Autophagy, which was independently implicated in the genetic landscape of ASD and IBD, was chosen during the first step of our methodology to be the case in point (i.e., PC).

Autophagy [7–9] is an evolutionarily conserved process in eukaryotes in which a double-membraned vesicle is formed in the cytosol and encloses its cargo, i.e., cytosolic material such as damaged organelles, protein aggregates and pathogens aimed for degradation. During steady-state conditions, this process maintains intracellular homeostasis in the various tissues through the elimination of damaged or old organelles and the turnover of long-lived proteins and protein aggregates. During stress conditions such as nutrient starvation, hypoxia, ER stress, oxidative stress and pathogen infection, autophagy can be upregulated, resulting in adaptation and cell survival. Neuronal autophagy is essential for development and neuronal signaling due to its important role in degrading toxic proteins and damaged organelles [7].

Autophagy was formerly considered to be a nonselective bulk degradation pathway; however, more recently selective autophagy processes have been identified. Selectivity of autophagy is controlled by autophagy receptors to specifically degrade intracellular ubiquitinated aggregates, bacteria, specific organelles or nucleic acids [10]. For example, the autophagy process plays a crucial role in immunity and inflammation, e.g., during cytosolic pathogenic degradation [11]. In addition, it is recognized that defective autophagy plays a significant role in human pathologies, including cancer, neurodegeneration, and infectious diseases [12].

The paper is structured as follows: the remainder of this section provides an overview of the target complex disease ASD, its comorbidity IBD and of SPN. Section 2 presents our methodology, including (1) our approach for translating literature-based knowledge into the SPN formalism, (2) the validation methods used and their significance, (3) the approach for the simulation's design, and (4) the way to make predictions based on different types of simulation results. Section 3 presents our results and predictions and demonstrates the feasibility of our CCS method. Section 4 concludes the paper.

1.1. The genetic-phenotypic relation of ASD/IBD

Autism spectrum disorder (ASD) is a neurodevelopmental disorder characterized by impairments in social interaction, repetitive behaviors and restricted interests [13] and affects about 1% of the population [14]. ASD is highly heritable [15,16] presenting an extremely heterogeneous genetic architecture [17], which connects to phenotype [18]. Rare SNPs (single-nucleotide polymorphisms)—changes in a single nucleotide and CNVs (Copy Number Variations) defined [19] as DNA segments that are 1 kb or larger in size present at variable copy number in comparison with a reference genome, that include insertion, deletion, duplication or other complex variation in the DNA [19]—have been frequently implicated in ASD [15].

ASD genetics that were recently related to the autophagy process include [15] small (<30 kb) rare deletions of the ATG7 autophagy gene and rare exonic CNV in the CALCOCO2/NDP52 autophagy receptor. In support of a role for the ATG7 gene and autophagy dysregulation in ASD etiology, a recent study [20] showed that a mouse model with cortical neuron-specific deletion of the autophagy gene *Atg7* (*Atg7*^{CKO} mice) had decreased pruning of dendritic spines and ASD-like behavioral symptoms.

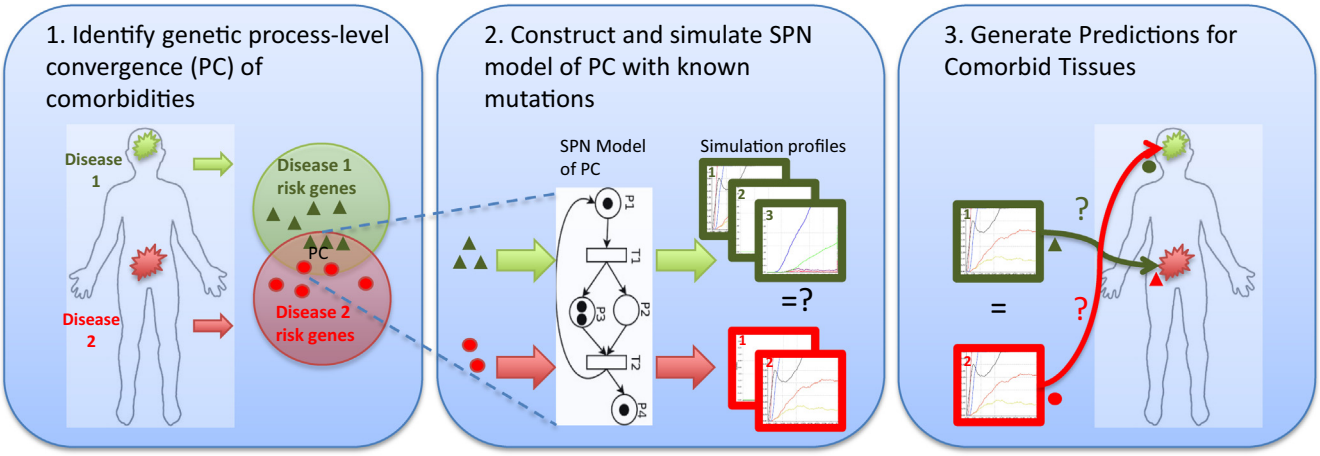

Fig. 1. CCS: a model-driven methodology to explore common molecular mechanisms ("process-level convergence" – PC) and predict new genes for complex disease comorbidities.

While ASD is considered to be a disorder of the developing brain, new evidence shows that comorbidities that affect other organs are frequently observed in patients with ASD [21,22]. These ASD-related comorbidities were suggested to cluster into four distinct groups [21] characterized by seizures, multisystem disorders including gastrointestinal disorders (GI), auditory disorders and infections, and psychiatric disorders. GI and IBD were shown [22] in over 14,000 autistic patients to be higher than in the general population (11.74% vs. 4.5% and 0.83% vs. 0.54% respectively). IBD is a chronic inflammatory disease of the digestive system that includes Crohn's disease and ulcerative colitis. Further research has shown IBD to occur at a higher rate in individuals with ASD [22–25] than in healthy cohorts.

The link between autophagy and IBD arose from genome-wide association studies (GWAS) that revealed several risk loci and SNPs in genes that are involved in autophagy [reviewed in 26] such as ATG16L1 [27–31], IRGM [27–29,32,33], NOD2 [27], ULK1 [34], ATG2A [35], GABARAPL1 [35] and NDP52/CALCOCO2 [36,37]. A large cohort of 3451 individuals [27] re-confirmed IRGM, NOD2 and ATG16L1 to be susceptible IBD genes that correlate to phenotype.

The functions of these specific autophagy-related risk loci were extensively studied in IBD. For example, the IBD-susceptible $ATG16L1^{T300A}$ risk locus in knock-in mice was shown to reduce autophagy in multiple cell types [38]. Deletion polymorphisms upstream of IRGM associated with Crohn's disease resulted in altered IRGM expression [33]. Cells homozygous for the Crohn's disease-associated NOD2 frameshift mutation (NOD2 p.L1007insC polymorphism) were defective in recruiting ATG16L1 to the plasma membrane and had a profound effect on the autophagic response triggered by intracellular bacterial infection [39].

Given that the process of autophagy is important in neuronal cellular cell survival [7] and its dysregulation is known to be implicated in a defective innate immune response in IBD [40], could the enrichment of IBD and ASD point to a subset of patients with a disordered autophagic system in common?

1.2. Stochastic Petri nets

A Petri net [4–6] is a discrete event simulation approach developed for system representation that enables concurrency and synchronization properties. This established formal and graphical technique abstracts systems dynamics with a graph composed of arcs and nodes, with tokens moving between the nodes. The structure of a Petri net is a directed bipartite graph with two types of nodes: places, which represent conditions (e.g., resources such as proteins), and transitions, which correspond to events that can change the state of the resources (e.g., molecular functions). A transition (an event) is connected to its input and output places with a weighted arc, whose default is 1. Input and output places represent the pre-conditions (e.g., substrates of an enzymatic reaction) and post-conditions (e.g., products) of the transition, respectively. Places are graphically drawn as circles, and transitions as bars or boxes. The state of the system (called marking) is represented by tokens that are positioned in the places; one place may hold multiple tokens. Thus, different assignments of tokens to places induce different states of the system (e.g., number of molecules representing a protein in a certain activation state).

Transitions change the state of the system by firing (i.e., moving) tokens along arcs. A transition t is enabled if its preconditions are satisfied, i.e., the number of tokens in each of its input places, p_{input}, is greater than or equal to the weight of the arc between p_{input} and t. During simulation, one of the enabled transitions fires. When a transition t fires, it removes tokens from p_{input} and adds tokens to each output place p_{output} of t according to the weights of the arcs.

A stochastic Petri net (SPN) [4–6] incorporates the notion of time into a Petri net and allows for the representation of rates of biological reactions and processes. A transition is assigned with an exponentially-distributed random variable with a parameter that defines the firing rate, i.e., the delay between the enabling and the firing of the transition. For stochastic simulations that determine when and which transition will be firing next, the most widely used SPN simulation is based on the well-established Gillespie algorithm [41]. In this instance, the SPN simulation is based on defining number of tokens (e.g., molecules) at different places and stochastic rates of transition firing delays (e.g., molecular function rates), which must be set in advance.

Petri nets are well-suited for modeling the concurrent behavior of biochemical networks and have been used [42,5] to represent various biological pathways such as metabolic pathways and protein synthesis. Petri nets are appropriate for modeling biological systems qualitatively, when the kinetic coefficients and the flux rates are unknown [4,5]. The non-deterministic feature of stochastic Petri nets is used to cope with this incomplete data and to simulate the biological system at hand [43].

Various tools support the Petri nets formalism in model validation, verification and analysis (e.g., mutation analysis). Petri nets analysis tools enable static analysis of the Petri net topology, dynamic simulation-based analysis and model checking techniques aimed for model verification [4–6].

P-invariants may be used to validate mass conservation by identifying a set of network places in which the total amount of tokens is bounded and remains constant. This constrains the sum of tokens belonging to related components or the different states of a component that must be preserved to a constant. P-invariants are calculated by solving the following system of linear equations: $C^T \cdot y = 0$, whereby y is a p-invariant. $C = [c_{ij}]_{n \times m}$, is an incidence matrix, where n is a number of places, m is a number of transitions. An entry c_{ij} in the incidence matrix C, is an integer number equal to the difference between the numbers of tokens present in place p_i ($i = 1,2,\ldots,n$, n is the number of net places) before and after transition t_j (for $j = 1,2,\ldots,m$, while m is number of net transitions) is fired. A Petri net covered by P-invariants (CPI) is a characteristic of a net where each place belongs to a P-invariant. A CPI net is a bounded net [4]. This is a desired property for modeling biological pathways where the total mass of molecules transformed throughout the pathway needs to stay bounded and conserved.

A T-invariant is a vector of integers corresponding to transitions that may fire to reproduce a given initial marking so that it detects cyclical behavior and may represent a biological pathway. Like P-invariants, T-invariants are calculated by solving the following system of linear equations: $C \cdot x = 0$ whereby x is a T-invariant, i.e., a vector of integers corresponding to transitions. A CTI [4,6] is a property of a network covered by T-invariants where each transition belongs to a support of a T-invariant. A CTI is an important property for the validation of a biological Petri net and can be used to validate unbounded nets. The CTI property examines that every transition, e.g., molecular function, in the net occurs in some subprocess and contributes to the steady behavior of the system. If the net does not fulfill the CTI property, the excluded transitions should be examined as a possible cause of tokens overflow in the net.

In addition to the static invariant analysis, simulating the SPN can be used to investigate the degree of process utilization as well as to analyze the states that the system reaches. Such dynamic analysis may be used to detect healthy conditions where equilibrium is reached or to detect disease conditions where oscillation occurs.

2. Methods

2.1. Step 1. Identifying genetic process-level convergence (PC) of comorbidities

First, a pair of comorbid complex diseases is identified and candidate-shared pathways are examined. We note that this step can be semi-automated. A fully automated process could be insufficient because, from our experience, some crucial data may be missed. For example, our attempt to automatically derive disease-related genes from known databases (e.g., MalaCards, a human disease database, http://www.malacards.org/, and SFARI, https://sfari.org/) resulted in missing one of the pivotal genes (i.e., ATG7) presented in this work.

2.2. Step 2. Model construction, simulation, and validation

Our SPN model was constructed manually based on the biological literature regarding the core autophagy mechanism [reviewed in 7–9] as presented in Section 3.2.1. We then extended the model with further mechanisms, presented with their references in Table 1 (column 1), that were required to model the ASD/IBD risk genes (e.g., ULK1, NOD2, IRGM, NDP52, GABARAPL1, CALCOCO2). The model was validated by domain experts who are co-authors (IK, AD, RS) of this paper.

Since the knowledge was incomplete, we included two conjectures in the model. One of the conjectures was related to IRGM, ATG16L1 and NOD2 that were shown to interact [44], while NOD1 and NOD2 was shown [39] to recruit ATG16L1 to the plasma membrane at bacterial entry. Since the temporal aspects of IRGM, ATG16L1 and NOD2 interactions are unknown (e.g., "does NOD2 bind IRGM and ATG16L1 after/before the autophagosome is formed?"), and ATG16L1 is known to be involved in autophagosome elongation phase, we conjectured that IRGM and NOD2 are required after autophagosome formation. Additionally, we modeled that GABARAPs and LC3 subfamilies are both required in recruiting selective receptors [reviewed in 45].

We used the Gene Ontology (GO) Consortium enrichment analysis tool (http://geneontology.org/) to evaluate the coverage of our model. Our model includes 37 participating genes/proteins and complexes. We mapped these genes to 44 human genes (see list in supplemental Table S5). Of these genes, 40 were mapped to the autophagy process. Conversely, using the GO annotation tool (http://www.ebi.ac.uk/QuickGO/), direct annotation of autophagy (GO: 0006914) includes 177 genes for humans (filtered with GO Identifier = "exact match" and Taxon = "human") and 141 genes for mice (filtered with GO Identifier = "exact match" and Taxon = "mouse"). Thus our model of the core autophagic machinery covers more than 20% of human direct autophagy genes/proteins as annotated by GO.

The Snoopy tool (Snoopy 2, version 1.13) [46] was used to construct and simulate the SPN model.

We used hierarchical structuring for managing the large-scale network by utilizing macro transitions. Macro transitions (drawn as two centric rectangles—see two such transitions in Fig. 3, top middle and bottom middle) permit us to manage the complexity of the net by using a scaling mechanism to define place-bordered subnets, i.e., subnets having only places as an interface to the supernet.

For referring to the same place in different subnets we used logical nodes. These are places (colored gray) that are logically identical whenever used through the network's distinct parts.

We used input transitions—transitions without input places that are therefore continuously enabled—to initiate the places in the net with tokens; and we used output transitions—transitions without output places that consume tokens and do not produce any tokens when fired—for modeling degradation of the modeled molecule/process. By default, the weights of all arcs equal one.

2.2.1. Structural model validation

A network that is re-initiated periodically by transitions in a recurring manner, is unbounded i.e., there is no finite upper bound on the total token number in the net. Such an unbounded net was suggested [47] to be valid by using the CTI feature, but does not obey the CPI (covered by p-invariants) feature which validates bounded nets. Thus in our model, CTI analysis validates that the initial state of the net can be restored and all tokens will be consumed after each execution cycle of the autophagy process.

The Charlie analysis tool (Charlie, version v2.0.194.229) [48] was used to perform structural net analysis. We refined our SPN model until it was fully covered by 1 minimal T-invariant (CTI), such that it represented a full pathway. Minimal T-invariants cannot be further decomposed into smaller T-invariants.

There are five bounded subnets in the net, which correspond to mass conservation (e.g., Beclin 1 to BCL2 – BCLXL complex assembly and disassembly) or recurring states of a molecule (e.g., activation and deactivation of ULK1). These subnets were validated to form P-invariants (presented in supplemental Table S3) and need to be initiated with a token.

2.2.2. Model simulation

We used a stochastic simulation to (1) further validate the model to comply with known experiments and (2) to compare the dynamic behavior over time as influenced by various LoF mutations. The firing time for a transition, e.g., an enzymatic reaction, is represented by a negative exponential distribution with the parameter λ. Due to the lack of more specific information, we assumed equal rates for all reactions, with the parameter $\lambda = 1$. These firing rates allow simulating the number of tokens in net places over time, which is measured in simulation time units. Therefore, our simulation is semi-quantitative because it does not relate to minutes or seconds. We defined the simulation interval to include 70 units, which was enough to show the trend (of these, we present an interval ending at 50 simulation time units in Fig. 6). We recorded 500 time points at this interval. Input/output transitions were calibrated and determined with $\lambda = 0.5$ and $\lambda = 0.25$ respectively in order to eliminate overflow of tokens in the net.

For all places in the net that represent the protein products of genes, one token represents a single molecule. Places are initiated during simulation by input transitions as explained above. Here too, the simulation is semi-quantitative because the number of tokens does not precisely reflect known cellular concentrations of molecules.

We analyzed the kinetic behavior of phagophores, autophagosomes, autolysosomes and the degraded cargo. These were chosen since they represent the products of autophagy stages and can be compared against experimental observations. For each product, such as autophagosomes, we count and show the quantity of the product at each simulation time point by subtracting the total number of products created and decayed. We summed up the number of tokens in the relevant net place (e.g., Autophagosome_Formed) over time and subtracted the number of degraded products represented by the AutophagosomeDegraded transition. These places are highlighted in Figs. 3–5.

Each LoF mutation was simulated independently and repeated 1000 times. The Snoopy 2 Petri net tool was used to show graphs of the averaged number of tokens in certain places of the net corresponding to autophagy stages as a function of time, representing the kinetic behavior.

Table 1
Dynamic model validation. Comparison of *in silico* and experimental observations regarding ASD/IBD risk genes.

Risk gene and their modeled function	Disease	Observed effects of gene deletion and specific risk loci on autophagy and disease phenotype (mutated genes are highlighted in "*Italic*" font)	*In silico* deletion effect on autophagy	*In silico* match known observation? (+/−)
ATG7. Mediates between ATG16L1 complex and LC3-II complex during autophagosome elongation [60 and as reviewed in 7–9]	ASD	A mouse model of *Atg7* deletion [60] showed that *Atg7* is essential for autophagosome formation and degradation of proteins and organelles. *Atg7* deficiency led to the appearance of concentric membranous structure and accumulation of ubiquitin-positive aggregates Observed effect on phenotype: Mice with cortical neuron–specific deletion of *Atg7* ($Atg7^{CKO}$ mice) had decreased pruning of dendritic spines and ASD-like behavioral symptoms. Deletion of *Atg7* in cultured primary hippocampal neurons also reduced spine pruning [20]	Phagophores and cargo accumulation, and reduced amounts of autophagosomes and autolysosomes (see Fig. 6B)	+
ATG16L1. Conjugates to ATG5, ATG12 and LC3-II and participates in autophagosome elongation [61 and as reviewed in 7–9]	IBD	*Atg16L1*-deficient cells resulted in severely impaired autophagosome formation and degradation of long-lived proteins [61] Observed risk locus effects on phenotype: T300A knock-in mice exhibit morphological defects in Paneth and goblet cells. Selective autophagy is reduced in multiple cell types from T300A knock-down in mice compared with WT mice. Moreover, $Atg16L1^{T300A}$ is associated with decreased antibacterial autophagy [38]	Phagophores accumulation, reduced levels of autophagosome, autolysosomes and accumulation of cargo (see Fig. 6C)	+
NOD52/CALCOCO2. A selective autophagy receptor that participates in immunity- autophagy that controls intracellular pathogens and binds the LC3 family in order to transport cargo into the autophagosomes before they bind to lysosomes [59]	IBD/ASD	*NDP52*-deficient autophagy of salmonella results in accumulation of autophagosomes [59]. *NDP52*-impaired cells facilitated bacterial proliferation and increased the number of cells containing ubiquitin-coated salmonella [62]	Phagophore and autophagosome accumulation, autolysosome reduction, decreased cargo degradation (pathogens) and thus increase in pathogens that were not degraded (see Fig. 6D)	+
IRGM. IRGM is essential for autophagy induction via associating with ULK1 and IRGM [44]	IBD	*IRGM* knock-down in monocytic cells reduced the total amount of ULK1 and ATG14L, autophagy initiation proteins, and decreased the levels of the activated form of AMPK phosphorylated at Thr-172, which is linked to autophagy induction [44] Observed risk locus effects: Deletion polymorphism upstream of *IRGM* associated Crohn's disease were linked with altered *IRGM* expression [33]	Reduced phagophores, autophagosomes and autolysosomes Reduced degraded cargo (see Fig. 6E and supplemental Fig. S1B)	+
NOD2. NOD2 is essential for autophagy induction via enhancing ULK1 and IRGM binding [44]	IBD	NOD2 enhances IRGM interactions with ULK1 and Beclin 1 for autophagy induction [44] Observed risk loci effects on phenotype: Dendritic cells (DCs) from individuals with Crohn's disease expressing Crohn's disease—associated *NOD2* risk variants (1007fsinsC, R702 W or G908R) are defective in autophagy induction, bacterial trafficking and antigen presentation [63]. Cells homozygous for the Crohn's disease-associated *NOD2* frameshift mutation (*NOD2* L1007insC polymorphism) were defective in recruiting ATG16L1 to the plasma membrane, and wrapping of invading bacteria by autophagosomes was impaired. It had a profound effect on the autophagic response triggered by intracellular bacterial infection [39].	Reduced phagophores (autophagy induction), autophagosomes and autolysosomes Reduced degraded cargo (increased undegraded bacteria) (see Fig. 6F and supplemental Fig. S1A)	+
ULK1. ULK1 is critical to induce the autophagic response, by activating ATG9, Ambra1 and PIK3C3 complex translocation to ER, Beclin 1 activation and ATG13 activation [64,65, as reviewed in 7–9]	IBD	The loss of *ULK1* and *ULK2* blocks nutrient deprivation-induced autophagy in mouse embryonic fibroblasts [65]. ULK1 is critical to induce the autophagic response of cerebellar granule neurons [65] Cells expressing the phosphorylation defective mutant, $Ulk1^{S317/777A}$, were deficient in autophagosome/autolysosome formation [64].	Reduced phagophores (autophagy induction), autophagosomes and autolysosomes Reduced and degraded cargo (see Fig. 6G)	+

Table 1 (*continued*)

Risk gene and their modeled function	Disease	Observed effects of gene deletion and specific risk loci on autophagy and disease phenotype (mutated genes are highlighted in "*Italic*" font)	*In silico* deletion effect on autophagy	*In silico* match known observation? (+/−)
GABARAPL1. GABARAPs subfamily functions as LC3 subfamily [reviewed in 45] GABARAPs subfamily involved in closure of autophagosome after they are elongated [57]	IBD	GABARAPs are localized to starvation-induced autophagosomes [68]. GABARAPs were shown to participate in a later stage of autophagosome formation, after elongation. Knocked-down *GABARAPs* affect the Atg5 and Atg16L1 structures, which appeared significantly larger (autophagosomes were formed) than in control cells [57]. Selective removal [57] of the *GABARAPs* subfamily leads to accumulation of open autophagic membranes, implying that GABARAPs are involved in the regulation of autophagosome maturation, which includes closure and sealing processes of the autophagosome	Phagophore and autophagosome accumulation, autolysosome reduction, decreased cargo degradation (see Fig. 6H)	+
ATG2A. ATG2A/B are recruited with WIPI proteins to form Atg2-WIPIs complex which binds the PI(3)P, before autophagosome elongation and before the phagophore is formed [66,67, as reviewed in 7–9]	IBD	Silencing of *Atg2A* and *Atg2B* causes a block in autophagic flux (LC3-II decrease—meaning a decreased autophagosome elongation, and p62 accumulation—meaning a decreased maturation to autolysosomes) and accumulation of unclosed autophagosome-related membranes [66] ATG2A/B are suggested to be recruited with WIPI proteins to form Atg2-WIPIs complex, which binds the PI(3)P, during autophagy initiation [66,67]	Reduced Phagophores, autophagosomes, autolysosomes and degraded cargo (see Fig. 6I)	+

2.2.3. Dynamic model validation

We executed the model after initializing it to reflect the setting of known experiments from the literature, and then determined whether our results comply with the published experimental results.

2.2.4. Modeling mutations

We analyzed the effects of mutations of ASD and IBD risk genes on our autophagy model. Our model granularity includes mutations at the gene level for disease risk genes characterized by various SNPs, rather than mutations of specific domains or alleles. The modeled mutations mimic partial loss of function mutations, i.e., gene product having less function. Partial loss of function was modeled as decrease in the quantities (number of tokens representing the gene) of the perturbed protein during simulation. To do so, we increased the weight of the arcs emanating from the place representing the protein. Using the simulation, we calibrated the weight of the arc until we received a significant effect on the system. We used a weight of 10 instead the default of 1 (a reduction to 10%) for all mutations.

We used the same model of the core autophagy mechanism to simulate both intestinal and neuronal cells because core autophagy is an evolutionarily-conserved mechanism that is thought to be similar for different cells types in general and specifically neuronal autophagy, as reviewed in [7].

We note that little is known about the phenotypic effects on autophagy of risk loci found in ASD and IBD. Nevertheless, the human polymorphism in ATG16L1 (rs2241880) that was linked to IBD was tested [38] by a knock-in mouse model expressing the *Atg16L1*^{T300A} variant resulting in decreased levels of full-length *Atg16Ll*^{T300A} proteins. In addition, Crohn's related deletions upstream of the IRGM gene (SNP rs13361189) were associated with altered IRGM expression [33]. Based on these findings, we mimic ASD/IBD genetic risk as decreased expression of the susceptible gene.

2.2.5. Availability of code for reproducibility

The model in supplemental SM1 allows full reproducibility of results.

2.3. Step 3. Generating predictions based on simulation results

We detected similar phenotypic effects by hierarchically clustering the eight kinetic plots, i.e., dynamic behavior over simulation time, of all simulations corresponding to the different perturbed risk genes. We recorded the accumulation of tokens in the three-autophagy vesicular stages—phagophores, autophagosomes, autolysosomes—and degraded cargo.

We stored the *in silico* kinetic results for each mutated gene in a vector. We then computed the Euclidian distance between these eight vectors and hierarchically clustered them. We used the clustering to predict similar groups of genes. We used the R software system for the computations.

As the network is not homogeneous with respect to its granularity, it would not be correct to test the distance between such vectors consisting of simulations of all net places. For example in comparing simulations of all net places, one may erroneously detect greater effect for genes with more detailed knowledge, meaning more net places affected by its perturbation.

The rationale for our comparative approach is that for an inherited mutation, the same gene in the same individual may affect autophagy in the same way but in different tissues, resulting in two distinct comorbidities. We detect such genes by comparing their phenotype, that is, the effect on autophagy products quantities over time, to be similar to the phenotype of genes known to be related to the comorbid disease. If particular kinetics were observed in gene$_1$ of disease$_1$ and in gene$_2$ of disease$_2$, then perhaps gene$_2$ could also cause this kinetic behavior that is typical for the manifestation of disease$_1$ in the tissue of disease$_1$. Therefore, if two independent genes are clustered together, we conjecture that each such gene may have a similar effect on the

comorbid tissue inducing the comorbid disease. Based on this clustering of model simulations, we suggest switching these identified genes between the diseases.

3. Results

3.1. Step 1. Selection of comorbidities and common process

ASD and its IBD comorbidity were chosen as a case in point. From a search of the literature, we found the common genetic architecture of ASD and IBD to converge at the pathway level of autophagy. This does not preclude other convergences, which we did not explore here.

3.2. Step 2. Autophagy model

3.2.1. The biology of autophagy

During the initiation of autophagy, the vesicle that starts forming is called a **phagophore**. During elongation, the phagophore forms a double membrane vesicle known as an **autophagosome**. The autophagosome later fuses with the lysosome to form an **autolysosome**, where its content is degraded. Autophagy-related (Atg) proteins function in multiprotein complexes that are involved in several continuous steps in autophagy including induction, vesicle nucleation, vesicle elongation and fusion of autophagosome with the lysosome (see Fig. 2). A central inhibitor of autophagy is the serine/threonine protein kinase mTOR (mechanistic target of rapamycin). mTOR negatively regulates autophagy by suppressing the function of the kinases ULK1 or ULK2. ULKs form a complex that contains FIP200 and ATG13 and is involved in autophagy induction. ULK1 may initiate autophagy by phosphorylating Beclin-1, then enhancing the activity of the ATG14L-containing VPS34 complexes [49]. Beclin-1 is also phosphorylated by death-associated protein kinase (DAPK) on its BH3 domain [50,51], which induces autophagy initiation by its release from its inhibitory binding partner Bcl-2. The Bcl-XL/Bcl-2 complex binds Beclin 1 via its BH3 domain to inhibit autophagy [52,53].

Upon autophagy induction, mTOR is inactivated, releasing ULKs from the inhibitory effect and subsequent autophagy induction [54]. Downstream to the ULK complex, the class III phosphatidylinositol 3-kinase (PI3K) complex functions to produce PI3P (phosphatidylinositol 3-phosphate) that regulates vesicle nucleation and subsequent recruitment of other factors such as WIPI1-2, ATG2 and DFCP1 that are involved in vesicle elongation. This complex is composed of the Vps34, Vps15/p150, Atg14 and Beclin 1 [55].

PI3K complex recruits two ubiquitin-like (Ubl) conjugation systems, Atg12–Atg5-Atg16 and LC3–PE (phosphatidylethanolamine), to the phagophore (initial sequestering compartment that expands into an autophagosome), and those complexes play an essential role in regulating the membrane elongation and expansion of the forming autophagosome [56]. In humans, LC3 is represented by two subfamilies [45]—the LC3-subfamily (LC3A, LC3B, LC3C) and the GABARAP subfamily (GABARAP, GABARAPL1, GABARAPL2, GATE-16). Both LC3 and the GABARAP subfamilies are essential for autophagy and were implicated in the membrane fusion of the autophagosomes as reviewed in [45]. During membrane elongation process, GABARAPs and LC3s are cleaved by ATG4 subfamily of enzymes into GABARAPL1-I, GABARAP-I, GABARAPL2-I and LC3-I which are conjugated to phospholipids by Atg7 and Atg3 to produce the phospholipid-linked forms GABARAPL1-II, GABARAP-II, GABARAPL2-II and LC3-II. LC3-II is required for elongation of autophagosomes, whereas GABARAP-II, GABARAPL1-II and GABARAPL2-II are required for later stages of [57] autophagosomes maturation.

Lastly, the autophagosome fuses with the lysosome and the **cargo** is degraded. Autophagosome-lysosome fusion is mediated by the same machinery that is involved in homotypic vacuole membrane fusion [58].

Selectivity of autophagy is controlled by autophagy receptors such as p62, NBR1, NDP52, OPTN, TOLLIP, Tax1BP1 and many others to specifically degrade intracellular ubiquitinated aggregates, bacteria, specific organelles or nucleic acids [10]. Specifically, IRGM which binds selective-immunity receptors was recently shown to regulate the formation of autophagy initiation complexes by interaction with ULK1 and Beclin 1 to enhance their co-assembly [44]. NOD2 was observed to enhance IRGM's interaction with ULK1 and Beclin1 [44]. IRGM [44] and NOD2 [39] form a complex with ATG16L1, while NOD2 translocates ATG16L1 to the cell membrane at the site of bacterial entry to induce selective autophagy. CALCOCO2/NDP52 [59] is an autophagy-selective receptor that regulates pathogen targeting to autophagosomes and subsequently ensures its degradation by regulating pathogen-containing autophagosome maturation and fusion with lysosomes.

3.2.2. SPN model

Our computational SPN model comprised more than 100 net places, 80 transitions and 200 arcs. All net places, transitions and their biological meaning are presented in supplemental Table S1 and S2. Fig. 3 depicts the top-level SPN, corresponding to the autophagy stages presented in Fig. 2, which are highlighted. The "Induction" stage is further expanded in subnet "Initiation" (see Fig. 4). "Vesicle Nucleation" stages are followed by the "Vesicle

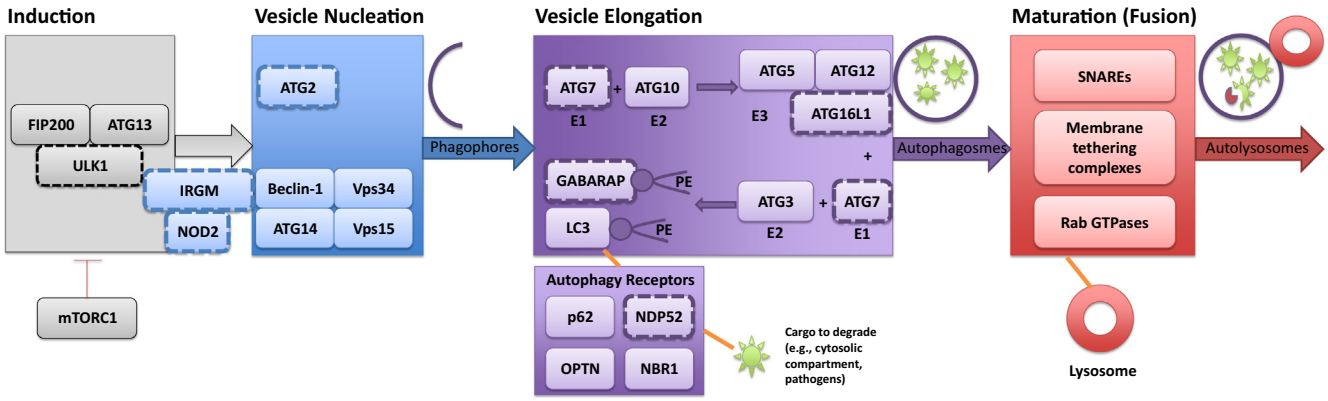

Fig. 2. Autophagy stages and main proteins. Genes related to ASD and IBD that we have perturbed *in silico* are highlighted with dashed lines. The state of the autophagy vesicle produced at each stage is depicted as text on the arrows connecting the stages.

Elongation" stage, which is further expanded in the "Autophago some_Elongation" subnet (see Fig. 5).

After constructing the model and before utilizing it for further analysis, we formally validated the model to be a CTI, fully covered by one minimal T-invariant (see Section 2 and supplemental Table S4). We also conducted P-invariants analysis and calculated five P-invariants (see supplemental Table S3). As explained in Section 2, due to the input transitions used to input tokens continuously into the net, we did not expect the SPN to be fully covered by P-invariants.

3.2.3. The in silico effects of ASD and IBD mutations

We used the SPN autophagy model simulation to analyze the effects of LoF mutations of the IBD risk genes, ATG16L1 [27–31], IRGM [27–29,32,33], NOD2 [27], ULK1 [34], NDP52/CALCOCO2 [36,37], ATG2A [35] and GABARAPL1 [35]. The latter two were related to Crohn's disease with granuloma [35]. In addition, we tested the ASD risk genes – ATG7 and ND52/CALCOCO2 [15]. These genes are highlighted by dashed rectangles in Fig. 2 and by dashed circles in the corresponding places in the SPN model in Figs. 3–5. Places that we analyzed in Fig. 6 are highlighted in Figs. 3–5 as well. The results of validation and prediction related to these genes are described below.

3.2.4. Dynamic model validation

Our simulation results are shown in Fig. 6. Table 1 summarizes these *in silico* results (see column 4) and their correspondence to observations (see columns 3 and 5). We also summarize the knowledge we modeled for each gene (see column 1). We summarized observed effects on autophagy and on disease phenotype of the risk gene/locus (see column 3).

ATG7 and ATG16L1 are thought to have a pivotal role in the general autophagy process, while the receptors NOD52/CALCOCO2, IRGM, NOD2 were shown to participate in selective autophagy to eliminate cytosolic pathogens [39,44,59,62,63]. That is, our analysis regarding these receptors pertains to the effects on selective immune-related autophagy rather than on general autophagy.

3.3. Step 3. Predictions generation

Next we focused on detecting genes/proteins with similar simulation profiles. Fig. 7 shows the results of hierarchical clustering of the differences between simulations (see Section 2). As expected, the clustering shows that a WT (wild type) simulation is a distinct group from the perturbed simulations. Between them, ATG2, ULK1, NOD2 and IRGM form one close group and GABARAPL1, NDP52, ATG16L1 and ATG7 form a second group. Within this second group (highlighted by dashed line), which is of interest because it includes both ASD and IBD risk genes, ATG16L1 and ATG7 genes show similar kinetic profiles (see Fig. 7). Based on the strongest similarity between ATG7 and ATG16L1, we predict that ATG16L1 (an IBD gene) may induce ASD when implicated in neurons; and ATG7 (an ASD gene) may induce IBD when implicated in the intestine epithelium.

We explored the literature and found results supporting our prediction that the ASD risk gene ATG7 has similar phenotypic effects to ATG16L1 in the intestine. ATG16L1 is the most studied susceptibility gene of IBD [27–31], and the work in [38] showed that the IBD risk locus in knock-in mice, *Atg16L1*^{T300A}, affects intestinal phenotype and exhibit morphological defects in Paneth and goblet cells. The work in [69] showed that mice with intestinal epithelial deletion of *Atg7* affect the intestinal phenotype. This phenotype included reduced size of granules and decreased levels of

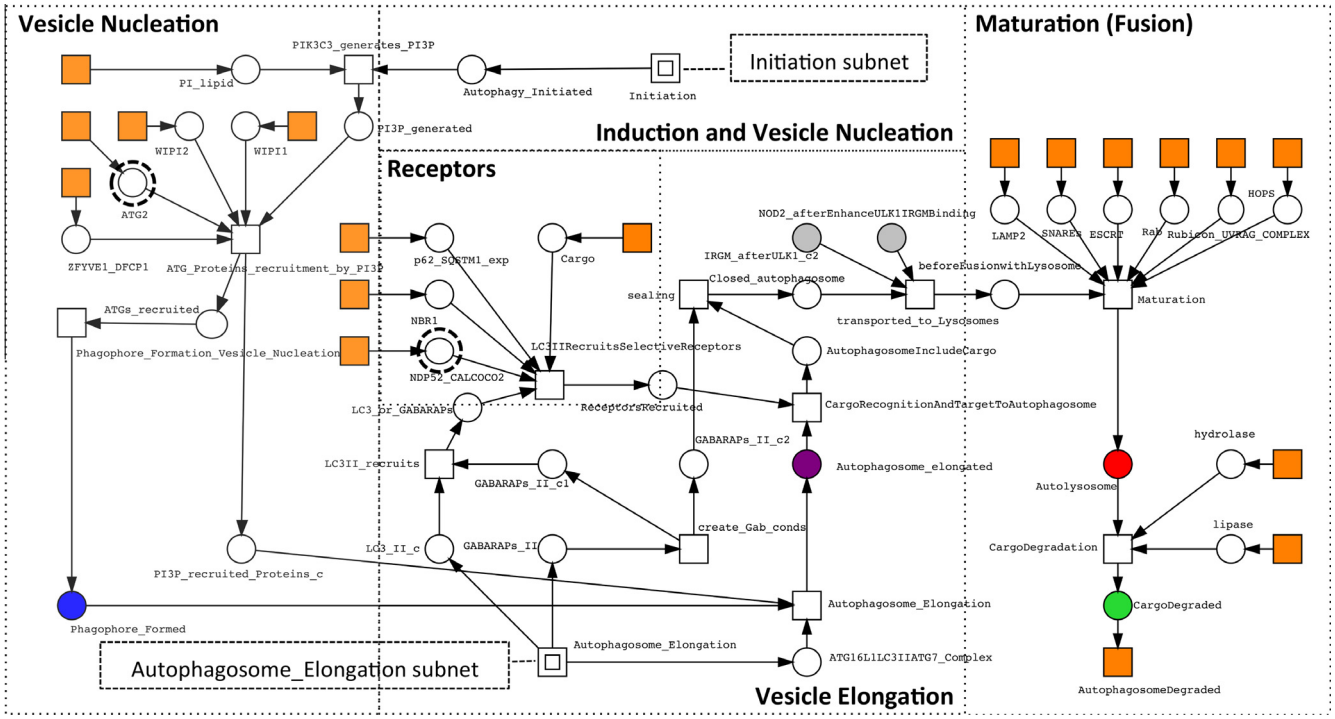

Fig. 3. Top-level view of the autophagy model. The four autophagy stages from Fig. 2 are highlighted. The "Induction" stage and part of the "Vesicle Nucleation" stage are further expanded in subnet "Initiation" (see Fig. 4). The "Vesicle Nucleation" stage is followed by the "Vesicle Elongation" stage, which is further expanded in the "Autophagosome_Elongation" subnet (see Fig. 5). The process starts in the top middle and ends with the "Maturation" stage. Circles depict places and rectangles depict transitions. Two concentric rectangles depict a macro transition, which represents a subnet. We highlighted the rectangles that represent input and output transitions, aimed at initiating places (e.g., proteins) with tokens (e.g., quantities). Gray circles represent logical places that participate also in other subnets. Places corresponding to our analysis in Fig. 6 are highlighted, such as Phagophore_formed, as well as the mutations that we tested highlighted by dashed circles. Shorthand used in names of places in Figs. 3–5: a_c/active_c – active as condition; AminoAcids_2 – Amino acids as condition 2; c – as condition; d/D – dephosphorylated; p/phos – phosphorylated; P_81 – dummy place.

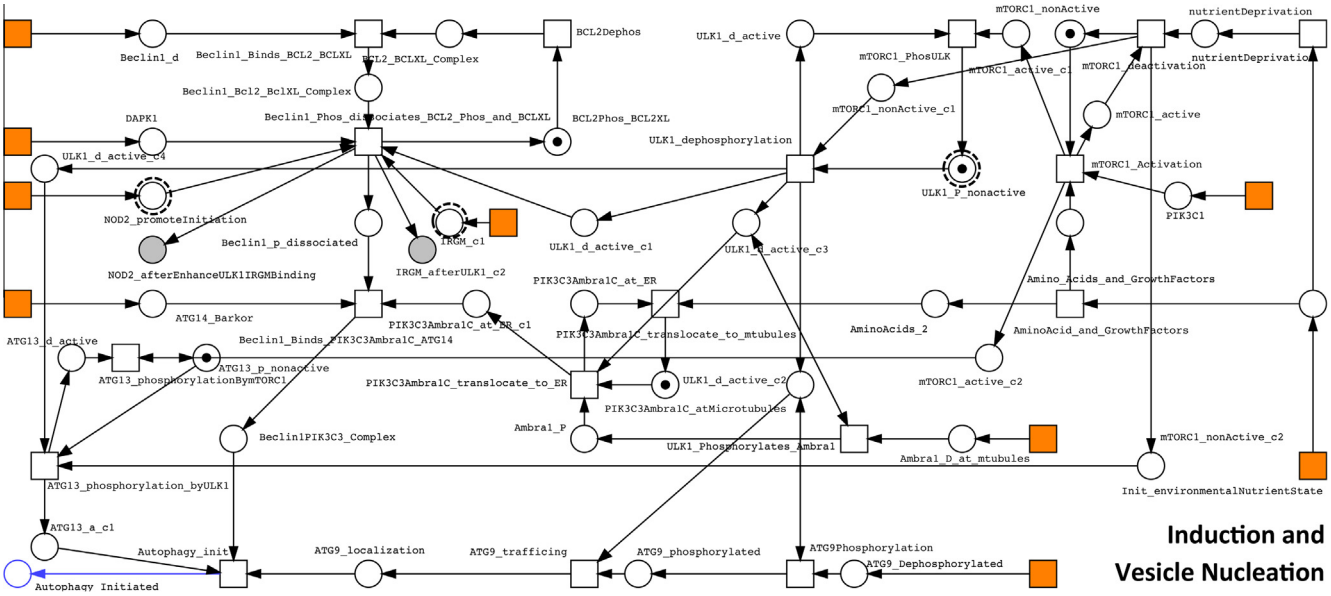

Fig. 4. The "Initiation" subnet presenting the "Induction" stage and part of the "Vesicle Nucleation" stage. The blue colored place and arc represent the border connection, linking the subnet to the upper level net. The genes that were analyzed are highlighted by dashed circles. (For interpretation of the references to color in this figure legend, the reader is referred to the web version of this article.)

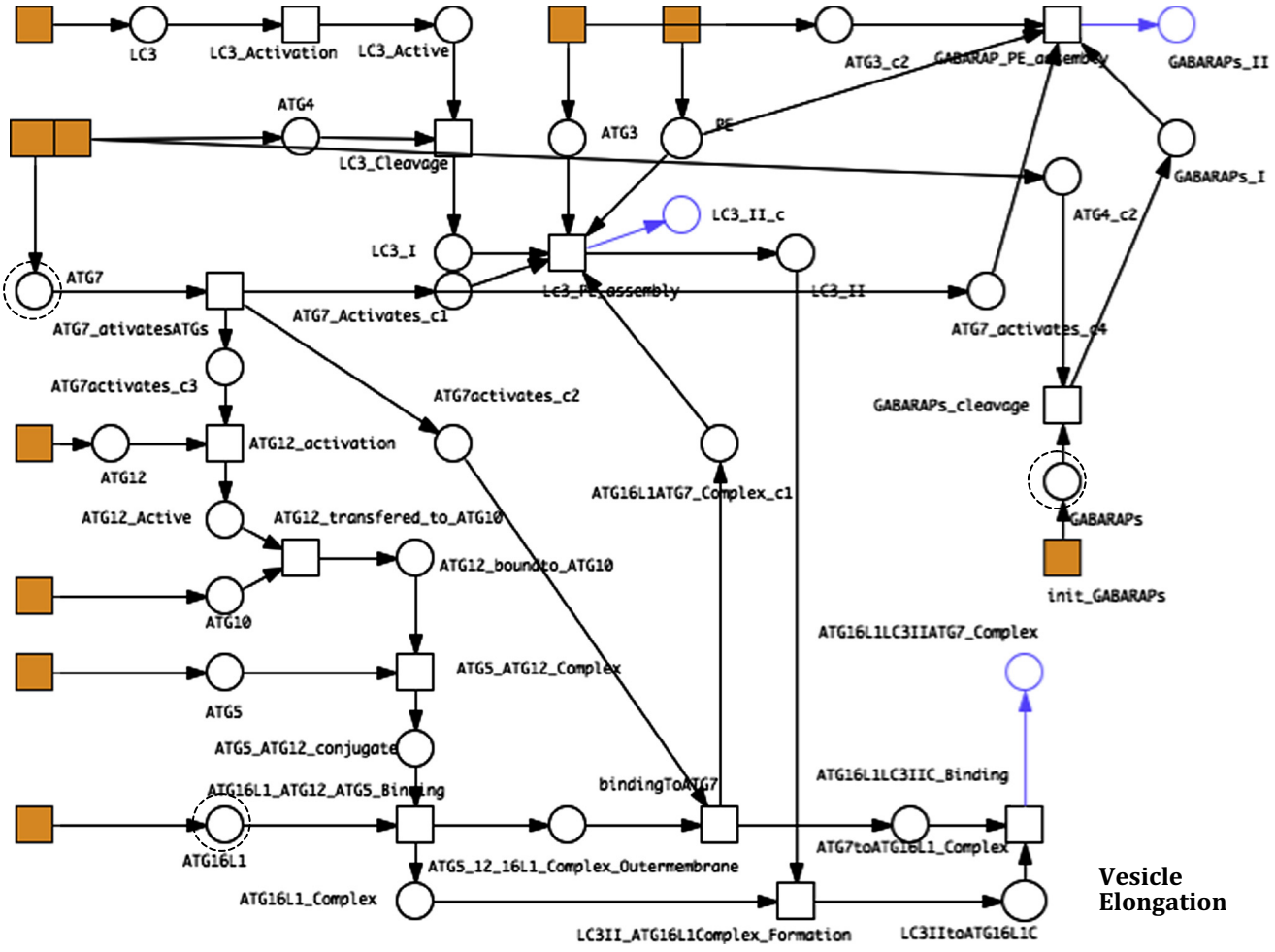

Fig. 5. Autophagosome_Elongation subnet presenting the "Vesicle Elongation" stage. The blue colored places and arcs represent the border connection, linking the subnet to the upper level net. The genes that were analyzed are highlighted by dashed circles. (For interpretation of the references to color in this figure legend, the reader is referred to the web version of this article.)

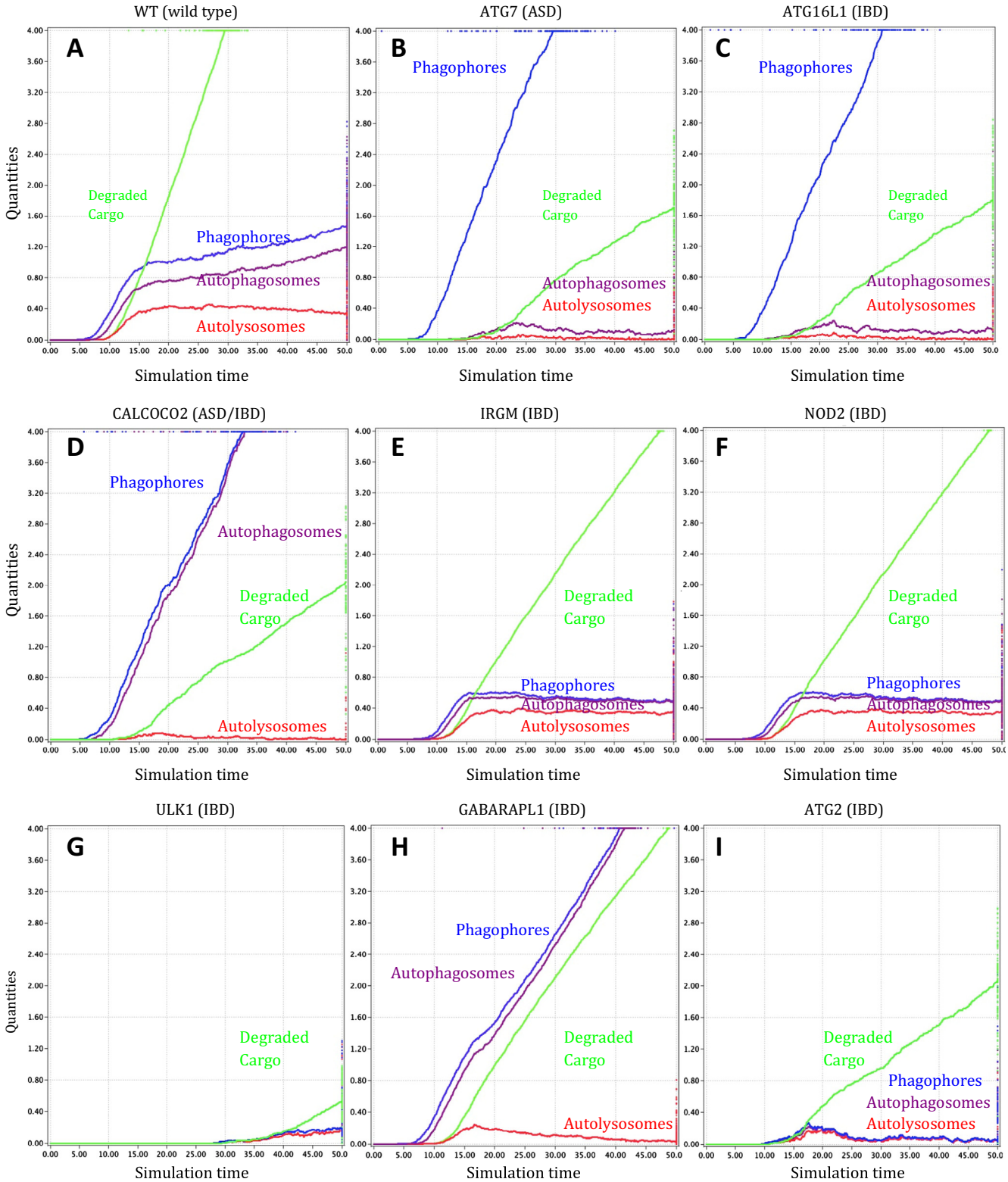

Fig. 6. *In silico* analysis of ASD and IBD risk genes modeled as partial LoF mutations, implicated in autophagy. The plots present the accumulation of tokens in places corresponding to the products of the three stages of the autophagy process (phagophores, autophagosomes, autolysosomes) and degraded cargo, corresponding to Fig. 2 and the marked places in Figs. 3–5. (A) Baseline simulation representing a wild type (WT) cell. (B) ATG7 mutation simulation, ASD risk gene. (C) ATG16L1 mutation simulation, IBD risk gene. (D) NDP52/CALCOCO2 mutation simulation, ASD and IBD risk gene. (E) IRGM mutation simulation, IBD risk gene. (F) NOD2 mutation simulation, IBD risk gene. (G) ULK1 mutation simulation, IBD risk gene. (H) GABARAPL1 mutation simulation, IBD risk gene. (I) ATG2 mutation simulation, IBD risk gene. We modeled genetic polymorphism and CNV as partial LoF mutation resulting in decreased levels of the risk genes (see Section 2). The *y*-axis shows the values of the performance measures (average number of tokens of 1000 simulations at certain places) from time zero to a given time on the *x*-axis. These kinetic curves use a smoothing function, which does not measure the number of tokens at a given time but rather the average number of tokens over a time interval.

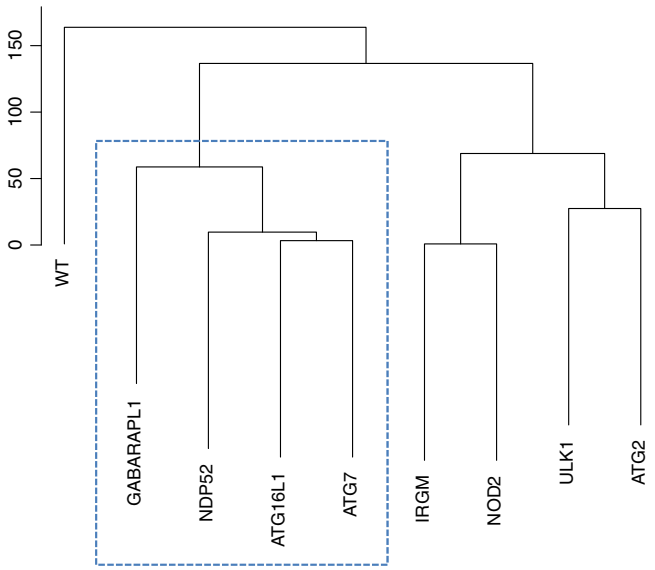

Fig. 7. Hierarchical clustered dendrogram of simulation results of ASD/IBD related mutations. The clustering is based on the *in silico* kinetics of phagophores, autophagosomes, autolysosomes and degraded cargo (see Fig. 6) resulting from LoF mutations of GABARAPL1, NDP52, ATG16L1, ATG7, IRGM, NOD2, ULK1, ATG2 and WT (wild type). It can be seen than the WT forms a distinct group from mutations. GABARAPL1 (IBD gene), NDP52 (ASD gene and IBD gene), ATG16L1 (IBD gene) and ATG7 (ASD gene) are clustered as one group and highlighted at the left. Within this group, ATG7 (ASD gene) and ATG16L1 (IBD gene) are clustered together. All the genes of the distinct group located at the right are IBD genes and were not included in our prediction.

lysozyme in Paneth cells. Also, mice with *Atg7* deficiency in intestinal epithelial cells develop more severe colitis upon infection with *Citrobacter rodentium* and reduced clearance of the pathogen [70].

Our results also predict similar effects in the NDP52/CALCOCO2 gene classified in the second group (see Fig. 7), which is shown to be susceptible in both ASD [15] and in IBD [36,37].

We also predict that perturbation of GABARAPL1 (an IBD risk gene), which is classified in the second group in Fig. 7, may also cause ASD, when implicated in neurons. Indeed GABARAPL1 has a role in neuronal signal transmission and was suggested to play a role in neurodegenerative diseases as reviewed in [45].

4. Discussion

Our novel approach leverages clinically-observed comorbidities to improve our understanding of the underlying mechanisms of complex disorders. It uses stochastic molecular level modeling to examine how genes implicated in a specific complex disease may impact its comorbid condition(s) and vice versa. The application of our approach to the ASD-IBD comorbidity has identified several genes previously implicated in one of the disorders that might affect both phenotypes or result in phenotypes shared in both diseases. Specifically, we predict that two IBD-implicated genes (ATG16L1 and GABARAPL1) may induce the ASD phenotype, and that one ASD-implicated gene (ATG7) may induce the IBD phenotype. We found support for our predictions regarding ATG7 [69,70] and GABARAPL1 [45]. Direct genomic and functional experiments can now test these predictions regarding the molecular basis of ASD and IBD.

The close similarity of the *in silico* profiles of ATG16L1 and ATG7 (see Fig. 7) can be explained by the tight connectivity of these genes. ATG16L1 and ATG7 are both involved in the elongation phase of autophagy during which the autophagosomes are formed (see Table 1, column1). Although ATG7 exhibits earlier roles than ATG16L1 during elongation, our model predicts that it affects autophagy products in a similar manner as the latter. GABARAPL1 and NDP52, which also cluster together with ATG16L1 and ATG7, are involved in later stages of the elongation phase and autophagosome maturation (see Table 1, column1). Another set of related genes, IRGM and NOD2, form a complex during autophagy initiation phase and are classified together. They are clustered with ULK1 and ATG2, which both affects the earlier stages of initiation and induction of autophagy (see Table 1, column1).

The strength of our approach is that by being comparative and qualitative, it is less sensitive to the magnitude of molecular quantities and rates used. This is necessary since these data (i.e., the exact coefficients, quantities and rate of the molecular reactions) are usually unknown for such complex biological systems.

Our model can be further used to test kinetics of other molecules and complexes of interest or effects of other mutations (or their combination) that may be present in real patients. We note that the granularity of our model is at the gene level and does not include specification of specific domains and risk loci. Future work may extend the granularity of our model and predict the effects of specific risk loci related to specific domains, when such data is available.

Our approach should be applicable to any pair of comorbid diseases that share genetic similarity, i.e., overlapping pathobiological mechanisms. Although our approach can handle incomplete knowledge, sufficient mechanistic knowledge about the biological process at hand and the genes to be tested is required. In addition, dedicated repositories of predefined computational models of biological processes can be used to ease the utilization of our approach. For example, the BioModels database (http://www.ebi.ac.uk/biomodels/) includes more than 140,000 freely available, manually curated and automatically generated models, as well as software tools for automated generation of mathematical models, derived from known pathway DBs (e.g., KEGG, BioCarta). The models are provided in the standard SBML format (Systems Biology Markup Language) [71], which may be imported into the Snoopy tool [46] that we have used in this work.

Although sharing high heritability, ASD and IBD are assumed to result from a complex interplay between genetic and environmental factors. Indeed, [38] showed that knock-down of the $Atg16L1^{T300A}$ IBD risk locus affected the intestine phenotype but did not evolve into spontaneous intestinal inflammation. Nevertheless, a combined genetic-environmental approach [72] shows that the *Atg16L1* susceptibility allele associated with viral exposure induces IBD. That is, while a solely genetic approach was not sufficient to trigger IBD [38], the combined genetic-environmental approach did. A related line of investigation [73] suggests that treating the gut-microbiota may improve the clinical state of children with ASD.

In summary, our study implicates genes, some for the first time, whose variants affect susceptibility to ASD and IBD. The study also explores the common mechanisms affected by the genetics of comorbid diseases. Finally, the study makes testable predictions regarding the common molecular behavior of the shared comorbidities.

Conflict of interest

Dr. Somekh has nothing to disclose.

Acknowledgments

This work was partially funded by the Conte Center for Computational Neuropsychiatric Genomics (NIH P50MH94267) for MP, SK, and IK.

Appendix A. Supplementary material

Supplementary data associated with this article can be found, in the online version, at http://dx.doi.org/10.1016/j.jbi.2016.08.008.

References

[1] R.D. Melamed, K.J. Emmett, C. Madubata, A. Rzhetsky, R. Rabadan, Genetic similarity between cancers and comorbid Mendelian diseases identifies candidate driver genes, Nat. Commun. 6 (2015) 7033, http://dx.doi.org/10.1038/ncomms8033.

[2] J. Park, D.-S. Lee, N.A. Christakis, A.-L. Barabási, The impact of cellular networks on disease comorbidity, Mol. Syst. Biol. 5 (2009) 262, http://dx.doi.org/10.1038/msb.2009.16.

[3] J. Menche, A. Sharma, M. Kitsak, et al., Disease networks. Uncovering disease-disease relationships through the incomplete interactome, Science 347 (6224) (2015) 1257601, http://dx.doi.org/10.1126/science.125760.

[4] M.A. Blätke, M. Heiner, W. Marwan, BioModel Engineering with Petri Nets, in: R. Robeva (Ed.), Algebraic and Discrete Mathematical Methods for Modern Biology, Elsevier Inc., 2015, pp. 141–193.

[5] M. Peleg, D. Rubin, R.B. Altman, Using Petri Net tools to study properties and dynamics of biological systems, J. Am. Med. Inform. Assoc. 12 (2) (2005) 181–199, http://dx.doi.org/10.1197/jamia.M1637.

[6] I. Koch, W. Reisig, F. Schreiber, Modeling in Systems Biology: The Petri Net Approach, first ed., Springer-Verlag New York, Inc., New York, NY, USA, 2011.

[7] K.-M. Lee, S.-K. Hwang, J.-A. Lee, Neuronal autophagy and neurodevelopmental disorders, Exp. Neurobiol. 22 (3) (2013) 133–142, http://dx.doi.org/10.5607/en.2013.22.3.133.

[8] Y. Feng, D. He, Z. Yao, D.J. Klionsky, The machinery of macroautophagy, Cell Res. 24 (1) (2014) 24–41, http://dx.doi.org/10.1038/cr.2013.168.

[9] C. He, D.J. Klionsky, Regulation mechanisms and signaling pathways of autophagy, Ann. Rev. Genet. 43 (2009) 67–93, http://dx.doi.org/10.1146/annurev-genet-102808-114910.

[10] A. Khaminets, C. Behl, I. Dikic, Ubiquitin-dependent and independent signals in selective autophagy, Trends Cell Biol. 26 (1) (2015) 6–16, http://dx.doi.org/10.1016/j.tcb.2015.08.010.

[11] B. Levine, N. Mizushima, H. Virgin, Autophagy in immunity and inflammation, Nature 469 (7330) (2011) 323–335, http://dx.doi.org/10.1038/nature09782.

[12] N. Mizushima, B. Levine, A.M. Cuervo, D.J. Klionsky, Autophagy fights disease through cellular self-digestion, Nature 451 (7182) (2008) 1069–1075, http://dx.doi.org/10.1038/nature06639.

[13] American Psychiatric Association. Diagnostic and statistical manual of mental disorders: (DSM-5®). American Psychiatric Pub, 2013. http://dx.doi.org/10.1176/appi.books.9780890425596.

[14] M. Elsabbagh, G. Divan, Y.-J. Koh, et al., Global prevalence of autism and other pervasive developmental disorders, Autism Res. 5 (3) (2012) 160–179, http://dx.doi.org/10.1002/aur.239.

[15] C.S. Poultney, A.P. Goldberg, E. Drapeau, et al., Identification of small exonic CNV from whole-exome sequence data and application to autism spectrum disorder, Am. J. Hum. Genet. 93 (4) (2013) 607–619, http://dx.doi.org/10.1016/j.ajhg.2013.09.001.

[16] G. Huguet, E. Ey, T. Bourgeron, The genetic landscapes of autism spectrum disorders, Annu. Rev. Genomics Hum. Genet. 14 (2013) 191–213, http://dx.doi.org/10.1146/annurev-genom-091212-153431.

[17] B.S. Abrahams, D.H. Geschwind, Advances in autism genetics: on the threshold of a new neurobiology, Nat. Rev. Genet. 9 (5) (2008) 341–355, http://dx.doi.org/10.1038/nrg2346.

[18] J. Chang, S.R. Gilman, A.H. Chiang, S.J. Sanders, D. Vitkup, Genotype to phenotype relationships in autism spectrum disorders, Nat. Neurosci. 18 (2) (2015) 191–198, http://dx.doi.org/10.1038/nn.3907.

[19] R. Redon, S. Ishikawa, K.R. Fitch, et al., Global variation in copy number in the human genome, Nature 444 (7118) (2006) 444–454, http://dx.doi.org/10.1038/nature05329.

[20] G. Tang, K. Gudsnuk, S.-H. Kuo, et al., Loss of mTOR-dependent macroautophagy causes autistic-like synaptic pruning deficits, Neuron 83 (5) (2014) 1131–1143, http://dx.doi.org/10.1016/j.neuron.2014.07.040.

[21] F. Doshi-Velez, Y. Ge, I. Kohane, Comorbidity clusters in autism spectrum disorders: an electronic health record time-series analysis, Pediatrics 133 (1) (2014) e54–e63, http://dx.doi.org/10.1542/peds.2013-0819.

[22] I.S. Kohane, A. McMurry, G. Weber, et al., The co-morbidity burden of children and young adults with autism spectrum disorders, PLoS One 7 (4) (2012) e33224, http://dx.doi.org/10.1371/journal.pone.0033224.

[23] K. Horvath, J.A. Perman, Autistic disorder and gastrointestinal disease, Curr. Opin. Pediatr. 14 (5) (2002) 583–587.

[24] M. Valicenti-McDermott, K. McVicar, I. Rapin, B.K. Wershil, H. Cohen, S. Shinnar, Frequency of gastrointestinal symptoms in children with autistic spectrum disorders and association with family history of autoimmune disease, J. Dev. Behav. Pediatr. 27 (2 suppl.) (2006) S128–S136. <http://www.ncbi.nlm.nih.gov/pubmed/16685179> (accessed June 22, 2015).

[25] F. Doshi-Velez, P. Avillach, N. Palmer, et al., Prevalence of inflammatory bowel disease among patients with autism spectrum disorders, Inflamm. Bowel Dis. 21 (10) (2015) 2281–2288, http://dx.doi.org/10.1097/MIB.0000000000000502.

[26] A. Gardet, R.J. Xavier, Common alleles that influence autophagy and the risk for inflammatory bowel disease, Curr. Opin. Immunol. 24 (5) (2012) 522–529, http://dx.doi.org/10.1016/j.coi.2012.08.001.

[27] E. Hoefkens, K. Nys, J.M. John, et al., Genetic association and functional role of Crohn disease risk alleles involved in microbial sensing, autophagy, and endoplasmic reticulum (ER) stress, Autophagy 9 (12) (2013) 2046–2055, http://dx.doi.org/10.4161/auto.26337.

[28] A. Franke, D.P.B. McGovern, J.C. Barrett, et al., Genome-wide meta-analysis increases to 71 the number of confirmed Crohn's disease susceptibility loci, Nat. Genet. 42 (12) (2010) 1118–1125, http://dx.doi.org/10.1038/ng.717.

[29] J.C. Barrett, S. Hansoul, D.L. Nicolae, et al., Genome-wide association defines more than 30 distinct susceptibility loci for Crohn's disease, Nat. Genet. 40 (8) (2008) 955–962, http://dx.doi.org/10.1038/ng.175.

[30] J.D. Rioux, R.J. Xavier, K.D. Taylor, et al., Genome-wide association study identifies new susceptibility loci for Crohn disease and implicates autophagy in disease pathogenesis, Nat. Genet. 39 (5) (2007) 596–604, http://dx.doi.org/10.1038/ng2032.

[31] J. Hampe, A. Franke, P. Rosenstiel, et al., A genome-wide association scan of nonsynonymous SNPs identifies a susceptibility variant for Crohn disease in ATG16L1, Nat. Genet. 39 (2) (2006) 207–211, http://dx.doi.org/10.1038/ng1954.

[32] M. Parkes, J.C. Barrett, N.J. Prescott, et al., Sequence variants in the autophagy gene IRGM and multiple other replicating loci contribute to Crohn's disease susceptibility, Nat. Genet. 39 (7) (2007) 830–832, http://dx.doi.org/10.1038/ng2061.

[33] S.A. McCarroll, A. Huett, P. Kuballa, et al., Deletion polymorphism upstream of IRGM associated with altered IRGM expression and Crohn's disease, Nat. Genet. 40 (9) (2008) 1107–1112, http://dx.doi.org/10.1038/ng.215.

[34] L. Henckaerts, I. Cleynen, M. Brinar, et al., Genetic variation in the autophagy gene ULK1 and risk of Crohn's disease, Inflamm. Bowel Dis. 17 (6) (2011) 1392–1397, http://dx.doi.org/10.1002/ibd.21486.

[35] M. Brinar, S. Vermeire, I. Cleynen, et al., Genetic variants in autophagy-related genes and granuloma formation in a cohort of surgically treated Crohn's disease patients, J. Crohns Colitis. 6 (1) (2012) 43–50, http://dx.doi.org/10.1016/j.crohns.2011.06.008.

[36] A. Till, S. Lipinski, D. Ellinghaus, et al., Autophagy receptor CALCOCO2/NDP52 takes center stage in Crohn disease, Autophagy 9 (8) (2013) 1256–1257, http://dx.doi.org/10.4161/auto.25483.

[37] D. Ellinghaus, H. Zhang, S. Zeissig, et al., Association between variants of PRDM1 and NDP52 and Crohn's disease, based on exome sequencing and functional studies, Gastroenterology 145 (2) (2013) 339–347, http://dx.doi.org/10.1053/j.gastro.2013.04.040.

[38] K.G. Lassen, P. Kuballa, K.L. Conway, et al., Atg16L1 T300A variant decreases selective autophagy resulting in altered cytokine signaling and decreased antibacterial defense, Proc. Natl. Acad. Sci. USA 111 (21) (2014) 7741–7746, http://dx.doi.org/10.1073/pnas.1407001111.

[39] L.H. Travassos, L.A.M. Carneiro, M. Ramjeet, et al., Nod1 and Nod2 direct autophagy by recruiting ATG16L1 to the plasma membrane at the site of bacterial entry, Nat. Immunol. 11 (1) (2010) 55–62, http://dx.doi.org/10.1038/ni.1823.

[40] R.J. Xavier, D.K. Podolsky, Unravelling the pathogenesis of inflammatory bowel disease, Nature 448 (7152) (2007) 427–434, http://dx.doi.org/10.1038/nature06005.

[41] D.T. Gillespie, Exact stochastic simulation of coupled chemical reactions, J. Phys. Chem. 81 (25) (1977) 2340–2361, http://dx.doi.org/10.1021/j100540a008.

[42] C. Chaouiya, Petri net modelling of biological networks, Brief Bioinform. 8 (4) (2007) 210–219, http://dx.doi.org/10.1093/bib/bbm029.

[43] L.J. Steggles, R. Banks, O. Shaw, A. Wipat, Qualitatively modelling and analysing genetic regulatory networks: a Petri net approach, Bioinformatics 23 (3) (2007) 336–343, http://dx.doi.org/10.1093/bioinformatics/btl596.

[44] S. Chauhan, M.A. Mandell, V. Deretic, IRGM governs the core autophagy machinery to conduct antimicrobial defense, Mol. Cell. 58 (3) (2015) 507–521, http://dx.doi.org/10.1016/j.molcel.2015.03.020.

[45] J.N. Le Grand, F.Z. Chakrama, S. Seguin-Py, et al., GABARAPL1 (GEC1): original or copycat?, Autophagy 7 (10) (2011) 1098–1107, http://dxdoi.org/10.4161/auto.7.10.15904.

[46] C. Rohr, W. Marwan, M. Heiner, Snoopy–a unifying Petri net framework to investigate biomolecular networks, Bioinformatics 26 (7) (2010) 974–975, http://dx.doi.org/10.1093/bioinformatics/btq050.

[47] M. Heiner, I. Koch, J. Will, Model validation of biological pathways using Petri nets–demonstrated for apoptosis, Biosystems 75 (1–3) (2004) 15–28, http://dx.doi.org/10.1016/j.biosystems.2004.03.003.

[48] M. Heiner, M. Schwarick, J. Wegener, Charlie – an extensible Petri net analysis tool, in: Proceedings of the PETRI NETS 2015, LNCS, vol. 9115, Springer, Brussels, 2015, pp. 200–211.

[49] R.C. Russell, Y. Tian, H. Yuan, et al., ULK1 induces autophagy by phosphorylating Beclin-1 and activating VPS34 lipid kinase, Nat. Cell Biol. 15 (7) (2013) 741–750, http://dx.doi.org/10.1038/ncb2757.

[50] E. Zalckvar, H. Berissi, L. Mizrachy, et al., DAP-kinase-mediated phosphorylation on the BH3 domain of beclin 1 promotes dissociation of beclin 1 from Bcl-XL and induction of autophagy, EMBO Rep. 10 (3) (2009) 285–292, http://dx.doi.org/10.1038/embor.2008.246.

[51] E. Zalckvar, H. Berissi, M. Eisenstein, A. Kimchi, Phosphorylation of Beclin 1 by DAP-kinase promotes autophagy by weakening its interactions with Bcl-2 and Bcl-X L, Autophagy 5 (5) (2014) 720–722, http://dx.doi.org/10.4161/auto.5.5.8625.

[52] M.C. Maiuri, G. Le Toumelin, A. Criollo, et al., Functional and physical interaction between Bcl-X(L) and a BH3-like domain in Beclin-1, EMBO J. 26 (10) (2007) 2527–2539, http://dx.doi.org/10.1038/sj.emboj.7601689.

[53] S. Pattingre, A. Tassa, X. Qu, et al., Bcl-2 antiapoptotic proteins inhibit Beclin 1-dependent autophagy, Cell 122 (6) (2005) 927–939, http://dx.doi.org/10.1016/j.cell.2005.07.002.
[54] P.-M. Wong, C. Puente, I.G. Ganley, X. Jiang, The ULK1 complex: sensing nutrient signals for autophagy activation, Autophagy 9 (2) (2013) 124–137, http://dx.doi.org/10.4161/auto.23323.
[55] M. Wirth, J. Joachim, S.A. Tooze, Autophagosome formation–the role of ULK1 and Beclin1-PI3KC3 complexes in setting the stage, Semin. Cancer Biol. 23 (5) (2013) 301–309, http://dx.doi.org/10.1016/j.semcancer.2013.05.007.
[56] J. Geng, D.J. Klionsky, The Atg8 and Atg12 ubiquitin-like conjugation systems in macroautophagy. "Protein modifications: beyond the usual suspects" review series, EMBO Rep. 9 (9) (2008) 859–864, http://dx.doi.org/10.1038/embor.2008.163.
[57] H. Weidberg, T. Shpilka, E. Shvets, Z. Elazar, Mammalian Atg8s: one is simply not enough, Autophagy 6 (6) (2010) 808–809, http://dx.doi.org/10.1038/emboj.2010.74.
[58] K. Moreau, M. Renna, D.C. Rubinsztein, Connections between SNAREs and autophagy, Trends Biochem. Sci. 38 (2) (2013) 57–63, http://dx.doi.org/10.1016/j.tibs.2012.11.004.
[59] P. Verlhac, I.P. Grégoire, O. Azocar, et al., Autophagy receptor NDP52 regulates pathogen-containing autophagosome maturation, Cell Host Microbe. 17 (4) (2015) 515–525, http://dx.doi.org/10.1016/j.chom.2015.02.008.
[60] M. Komatsu, S. Waguri, T. Ueno, et al., Impairment of starvation-induced and constitutive autophagy in Atg7-deficient mice, J. Cell Biol. 169 (3) (2005) 425–434, http://dx.doi.org/10.1083/jcb.200412022.
[61] T. Saitoh, N. Fujita, M.H. Jang, et al., Loss of the autophagy protein Atg16L1 enhances endotoxin-induced IL-1beta production, Nature 456 (7219) (2008) 264–268, http://dx.doi.org/10.1038/nature07383.
[62] T.L.M. Thurston, G. Ryzhakov, S. Bloor, N. von Muhlinen, F. Randow, The TBK1 adaptor and autophagy receptor NDP52 restricts the proliferation of ubiquitin-coated bacteria, Nat. Immunol. 10 (11) (2009) 1215–1221, http://dx.doi.org/10.1038/ni.1800.
[63] R. Cooney, J. Baker, O. Brain, et al., NOD2 stimulation induces autophagy in dendritic cells influencing bacterial handling and antigen presentation, Nat. Med. 16 (1) (2010) 90–97, http://dx.doi.org/10.1038/nm.2069.
[64] J. Kim, M. Kundu, B. Viollet, K.-L. Guan, AMPK and mTOR regulate autophagy through direct phosphorylation of Ulk1, Nat. Cell Biol. 13 (2) (2011) 132–141, http://dx.doi.org/10.1038/ncb2152.
[65] E.-J. Lee, C. Tournier, The requirement of uncoordinated 51-like kinase 1 (ULK1) and ULK2 in the regulation of autophagy, Autophagy 7 (7) (2011) 689–695, http://dx.doi.org/10.4161/auto.7.7.15450.
[66] A.K.G. Velikkakath, T. Nishimura, E. Oita, N. Ishihara, N. Mizushima, Mammalian Atg2 proteins are essential for autophagosome formation and important for regulation of size and distribution of lipid droplets, Mol. Biol. Cell. 23 (5) (2012) 896–909, http://dx.doi.org/10.1091/mbc.E11-09-0785.
[67] E. Itakura, N. Mizushima, Characterization of autophagosome formation site by a hierarchical analysis of mammalian Atg proteins, Autophagy 6 (6) (2010) 764–776, http://dx.doi.org/10.4161/auto.6.6.12709.
[68] Y. Kabeya, N. Mizushima, A. Yamamoto, S. Oshitani-Okamoto, Y. Ohsumi, T. Yoshimori, LC3, GABARAP and GATE16 localize to autophagosomal membrane depending on form-II formation, J. Cell Sci. 117 (Pt 13) (2004) 2805–2812, http://dx.doi.org/10.1242/jcs.01131.
[69] N. Wittkopf, C. Günther, E. Martini, et al., Lack of intestinal epithelial atg7 affects paneth cell granule formation but does not compromise immune homeostasis in the gut, Clin. Dev. Immunol. 2012 (2012) 278059, http://dx.doi.org/10.1155/2012/278059.
[70] J. Inoue, S. Nishiumi, Y. Fujishima, et al., Autophagy in the intestinal epithelium regulates Citrobacter rodentium infection, Arch. Biochem. Biophys. 521 (1–2) (2012) 95–101, http://dx.doi.org/10.1016/j.abb.2012.03.019.
[71] M. Hucka, A. Finney, H.M. Sauro, et al., The systems biology markup language (SBML): a medium for representation and exchange of biochemical network models, Bioinformatics 19 (4) (2003) 524–531, http://dx.doi.org/10.1093/bioinformatics/btg015.
[72] K. Cadwell, K.K. Patel, N.S. Maloney, et al., Virus-plus-susceptibility gene interaction determines Crohn's disease gene Atg16L1 phenotypes in intestine, Cell 141 (7) (2010) 1135–1145, http://dx.doi.org/10.1016/j.cell.2010.05.009.
[73] Q. Li, J.-M. Zhou, The microbiota-gut-brain axis and its potential therapeutic role in autism spectrum disorder, Neuroscience 324 (2016) 131–139, http://dx.doi.org/10.1016/j.neuroscience.2016.03.013.